A new mimetic scheme for the acoustic wave equation

F. Solano-Feo[a], J. M. Guevara-Jordan[a], O. Rojas[b], B. Otero[c], R. Rodriguez[d]

[a]*Escuela de Matemática, Facultad de Ciencias, Universidad Central de Venezuela, Caracas, Venezuela*
[b]*Escuela de Computación, Facultad de Ciencias, Universidad Central de Venezuela, Caracas, Venezuela*
[c]*Dpto. de Arquitectura d'Computadors, Universitat Politécnica de Catalunya, Campus Nord, Barcelona, Spain*
[d]*Escola Tècnica Superior d'Enginyeria de Telecomunicació de Barcelona, Universitat Politécnica de Catalunya, Barcelona, Spain*

Abstract

A new mimetic finite difference scheme for solving the acoustic wave equation is presented. It combines a novel second order tensor mimetic discretizations in space and a leapfrog approximation in time to produce an explicit multidimensional scheme. Convergence analysis of the new scheme on a staggered grid shows that it can take larger time steps than standard finite difference schemes based on ghost points formulation. A set of numerical test problems gives evidence of the versatility of the new mimetic scheme for handling general boundary conditions.

Keywords:
Tensor, mimetic, acoustic wave, convergence, staggered grid, boundary conditions, explicit scheme.

1. Introduction

Mimetic methods are a relatively new set of numerical techniques for solving partial differential equations (PDE's). They have been developed within the last twenty years and several formulations can be found in [1, 2, 3, 4]. All these versions provide discretizations for the main operators of mathematical physics: divergence, gradient, and curl, that satisfy discrete versions of Green-Gauss-Stokes' theorems. These discrete operators are later combined or composed to design mimetic schemes for approximating solutions of PDE's. Discrete mimetic operators proposed in [1] have the same order of accuracy at both interior and boundary grid nodes. On the other hand, formulations given in [2, 3, 4] lower the order of accuracy at boundary nodes. Thus, all schemes based on referred formulations are mimetic, but they are not numerically equivalent. This article is focused on mimetic operators developed in [1], which have been less applied than those described in [2, 3, 4].

Applications of mimetic methods to wave propagations problems have been widely reported in the literature. For instance, [4] in gas dynamics, [3, 5, 6] for Maxwell's equations , and [7, 8, 9, 10, 11] in geophysics. In particular, [4, 10] propose a second order mimetic scheme to the acoustic wave equation written as a first order system for the pressure and velocity fields. The convergence analysis of this method by using the Von Neumann's approach is discussed in [4], as part of a stability analysis for the gas dynamics equations. The same scheme is adapted to geophysical applications by [10] after including the perfectly matched layer approach for the absorption of outgoing waves. Second order mimetic schemes for the acoustic wave equation based on operators described in [1, 12, 13] have not been reported in the technical literature, in spite of higher order mimetic operators have been used on elastic applications [1, 7, 9]. The main purpose of this article is to formulate, analyze, and test a new second order mimetic scheme for the scalar acoustic wave equation based on operators given in [1, 12, 13]. We express the mimetic discretizations of gradient and divergence operators in a tensor form valid for any space dimension, which gives this new method a great generality. Although tensor products have been known for some time in the context of standard finite difference methods, [14, 15], their full introduction to mimetic methods is relatively new [1, 3].

This article has been divided into six sections. The first section is this introduction and bibliographical review. Then, the second section presents our discrete tensor formulation of mimetic gradient and divergence operators based

Email addresses: freysimar.solano@ciens.ucv.ve (F. Solano-Feo), jmguevarajordan@gmail.com (J. M. Guevara-Jordan), rojasotilio@gmail.com (O. Rojas), botero@ac.upc.edu (B. Otero), robert.rc47@gmail.com (R. Rodriguez)

on the Kronecker product of the one dimensional operators proposed in [12, 13]. Next, these tensor operators are used in the formulation of our new mimetic scheme for the acoustic wave equation in section three. The following section provides an analytic convergence analysis of the new scheme under periodic boundary conditions. The fifth section describes applications of this scheme to a set of test problems. Finally, the conclusions of this article are given in section six.

2. Mimetic operators

In this article all the mimetic discretizations are developed for uniform staggered grids. One dimensional second order mimetic discretizations for the gradient and divergence operators have been well documented in [1, 12, 13]. Their description will be briefly presented, for the sake of completeness, in reference to the one dimensional uniform staggered grid displayed in figure 1.

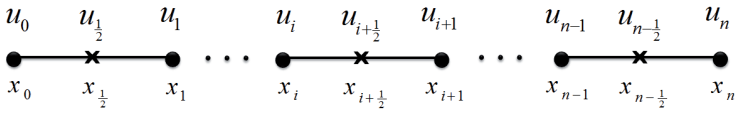

Figure 1: One dimensional staggered grid

In this figure, crosses represent block's centers and black circles are the block's edges. The one dimensional mimetic discretization of divergence operator is computed at the block's center by standard central difference $D_{1d}u_{i+\frac{1}{2}} \equiv \frac{u_{i+1}-u_i}{h}$ with $h \equiv x_{i+1} - x_i$. Its matrix's formulation will be denoted by D^n_{1d}, which includes two additional zero rows, the first and the last rows, to enforce consistency in matrix dimension. Gradient mimetic discretizations are defined at the block's edges by central finite differences $G_{1d}u_i \equiv \frac{u_{i+\frac{1}{2}}-u_{i-\frac{1}{2}}}{h}$, $h \equiv x_{i+\frac{1}{2}} - x_{i-\frac{1}{2}}$, in addition to one sided second order approximations at both boundary edges $G_{1d}u_0 \equiv \frac{-\frac{8}{3}u_0+3u_{\frac{1}{2}}-\frac{1}{3}u_{\frac{3}{2}}}{h}$, and $G_{1d}u_n \equiv \frac{\frac{8}{3}u_n-3u_{n-\frac{1}{2}}+\frac{1}{3}u_{n-\frac{3}{2}}}{h}$. The gradient matrix representation is denoted by G^n_{1d}. For the sake of clarity, we present the explicit forms of D^n_{1d} and G^n_{1d} in Appendix A. The upper index in both matrices denotes the grid dimension. From their definition, mimetic divergence and gradient operators allow second order accurate differentiation at all grid points. Higher dimensional mimetic discretizations of gradient and divergence operators can be systematically obtained from their one dimensional versions by using Kronecker's tensor product, denoted by $\otimes$, and defined in any of these references [1, 3, 14, 15]. In two dimensions the mimetic discretizations of the divergence operator on a $m \times n$ staggered grid is defined by the matrix

$$D^{m\times n}_{2d} \equiv \begin{pmatrix} I_n \otimes D^m_{1d} & D^n_{1d} \otimes I_m \end{pmatrix}. \tag{1}$$

In this matrix first entry represents the approximations of partial derivatives in the x direction, while the second entry are the approximations to derivatives in the y direction. A similar expression with a slightly different notation can be found in [1]. In the three dimensional case, the mimetic approximation to the divergence on a $m \times n \times k$ staggered grid is defined by

$$D^{m\times n\times k}_{3d} \equiv \begin{pmatrix} I_k \otimes I_n \otimes D^m_{1d} & I_k \otimes D^n_{1d} \otimes I_m & D^k_{1d} \otimes I_n \otimes I_m \end{pmatrix}. \tag{2}$$

This expression has an additional term to approximate partial derivatives in the z direction. It differs from the one given in [3] in various details. The matrix I_i, in (1) and (2), has dimension $i + 1 \times i$, its first and last rows are null, and rows between them are those of a i dimensional identity matrix. Mimetic discretization for the gradient operator on a $m \times n$ grid is given by the following expression

$$G^{m\times n}_{2d} \equiv \begin{pmatrix} I^t_n \otimes G^m_{1d} & G^n_{1d} \otimes I^t_m \end{pmatrix}^t, \tag{3}$$

where the upper subindex t denotes the transpose of a matrix, and I_i matrices have same description as in the divergence discretizations. The submatrix on the left represents the gradient component in the x direction, while the one on the right has the derivatives along the y direction. This mimetic discretization, with a small correction, is proposed in [1],

which is an adaptation of the one given in [3] for mimetic discretizations with a lower order of accuracy at boundaries. Extension of gradient mimetic discretization to three dimensional $m \times n \times k$ grid is defined by

$$G_{3d}^{m\times n\times k} \equiv \begin{pmatrix} I_k^t \otimes I_n^t \otimes G_{1d}^m & I_k^t \otimes G_{1d}^n \otimes I_m^t & G_{1d}^k \otimes I_n^t \otimes I_m^t \end{pmatrix}^t, \tag{4}$$

where the block component on the right represents the mimetic discretization of the gradient's third component in the z direction. Although this is a straightforward combination of the theories presented in [1, 3], it has not been previously reported in the literature. Mimetic discretizations (1), (2), (3), and (4) represent an elegant formulation that avoids explicit reference to higher dimensional grid ordering. In the case of divergence discretizations, (1) and (2) lead to a lexicographic grid ordering of center's and boundary nodes on the staggered grid. On the other hand, (3) and (4) order the x gradient edge nodes first, followed by the y gradient edge nodes, and finally the z gradient edge nodes, in the three dimensional case. The two dimensional case has the same described sequence, but omitting the ordering in z.

The above gradient and divergence mimetic discretizations satisfy a discrete versions of the Green-Gauss-Stokes' theorem, which takes the following form

$$\langle D_{nd}^s u, v\rangle_{h^n Q} + \langle G_{nd}^s u, v\rangle_{h^n P} = \langle B_{nd}^s u, v\rangle_{h^{n-1} I}. \tag{5}$$

In this equation, n represents the dimension, s is the grid size, and h is the grid's block size. The bracket $\langle\cdot,\cdot\rangle_A$ is a generalized inner product of the form $\langle u, v\rangle_A \equiv u^t A v$, where A is a matrix weight. Q and P are diagonal matrices whose entries are the weights of the midpoint quadrature, and of the $\frac{3}{8}$'s Newton Cotes quadrature, respectively. Matrix I corresponds to the identity matrix, and B_{nd}^s is the boundary operator. The general expression (5) is an original contribution of this article, from a notational point of view, that summarizes in a single equation the discrete version of Green-Gauss-Stokes' theorem for any space dimension ($n = 1, 2$, and 3). In the particular case of $n = 1$, equation (5) agrees with one dimensional expressions previously reported in the technical literature [1, 12, 13]. The Green-Gauss-Stokes' theorem (5) provides the following explicit expression for the boundary operator,

$$B_{nd}^s = hQD_{nd}^s + h(G_{nd}^s)^t P. \tag{6}$$

This result is an immediate consequence of the generalized inner product definition used in (5).

Mimetic operators D_{nd}^s, G_{nd}^s, and B_{nd}^s are the only ones required by the discretization of the acoustic wave equation. Their formulation and formal description in a general multidimensional context, represents an important advance in the development of mimetic method as described in [1, 12, 13].

3. Mimetic scheme

In this section, we present a new mimetic scheme for the acoustic wave equation, and assume the following model for this equation

$$\frac{1}{c^2}\frac{\partial^2 u}{\partial t^2} - \Delta u = f. \tag{7}$$

Parameter c is the wave's speed, u is the wave's amplitude, f is a source term, ∂ is a partial derivative, and Δ the Laplace's operator or laplacian. In this article, the wave speed may be constant or space dependent, thus equation (7) may represent either the homogeneous or the heterogeneous wave equation, respectively. The laplacian can be expressed as a composition of the divergence, $\nabla\cdot$, and the gradient, ∇, and then equation (7) can be written as

$$\frac{1}{c^2}\frac{\partial^2 u}{\partial t^2} - \nabla\cdot\nabla u = f. \tag{8}$$

Note that the acceleration term is also a one dimensional laplacian in time. Therefore, it can be decomposed as one dimensional divergence, $\nabla\cdot_t$, and gradient, ∇_t, operators in time. With this convention in mind, (7) can take the following form

$$\frac{1}{c^2}\nabla\cdot_t\nabla_t u - \nabla\cdot\nabla u = f. \tag{9}$$

This representation is very convenient for describing the mimetic scheme. If U_m represents the mimetic approximations to u, F and C^2 are the projections of f and c^2 on the staggered grid, and the continuous gradient and divergence operators in (9) are replaced by their mimetic approximations then the expression

$$\frac{1}{C^2}(D^{st}_{1d}G^{st}_{1d})_t U_m - D^s_{nd}G^s_{nd}U_m = F \tag{10}$$

represents a formal mimetic discretization of the acoustic wave equation with some dimension inconsistencies in matrices and vectors involved in this expresion. In addition, we need to adopt a time discretization scheme and assign appropriate time levels to U_m. This inconsistency can be easily solved by a convenient interpretation of (10) to formulate a numerical scheme. Let's denote by U^n_m to the mimetic approximation of u at the $n\triangle t$ time step, where $\triangle t$ is the time step size. The time discretization term in (10) provides all st time steps at once, but a correct interpretation is taking it as a time discretization at a generic time step, which leads to the leapfrog form $\frac{1}{C^2}\frac{(U^{n+1}_m - 2U^n_m + U^{n-1}_m)}{\triangle t^2}$. Here, $\frac{1}{C^2}$ is a diagonal matrix with $\frac{1}{c^2}$ at diagonal entries associated with block's centers in the staggered grid. In order to obtain an explicit scheme, the mimetic approximation U_m present in the spatial term and F in (10) must be evaluated at the n time step, i.e., U^n_m and F^n. These approximations combined to the leapfrog time discretization yields the following partial mimetic scheme for the acoustic wave equation

$$\frac{1}{C^2}\frac{(U^{n+1}_m - 2U^n_m + U^{n-1}_m)}{\triangle t^2} - D^s_{nd}G^s_{nd}U^n_m = F^n. \tag{11}$$

To complete the formulation of the new mimetic scheme, we need to add consistent boundary and initial conditions. Latter conditions give the position and velocity of u at $t = 0$. Their discretization is the standard one, based on the projection on the staggered and coupled to a forward finite difference in time, that provides approximations U^0_m and U^1_m both required for initialization of the numerical scheme.

Equation (7) can be solved on bounded or unbounded regions. In the former case, this equation requires of boundary conditions in addition to the initial ones to state a well posed bounded initial value problem [16]. Standard boundary conditions on bounded regions are Dirichlet's or Neumann's condition, which can be easily combined in a general Robin's condition

$$\beta\frac{\partial u}{\partial n} + \alpha u = h, \tag{12}$$

where β, α, and h must be known boundary functions [16]. Partial derivative respect to n represents the directional derivative respect to the exterior normal unitary vector on the boundary. If β or α is null then either a Dirichlet or a Neumann condition are obtained, respectively. The equation (7) under Robin's boundary conditions correspond to a well posed boundary initial value problem. Mimetic discretizations of (12) is

$$BB^s_{nd}G^s_{nd}U^n_m + AU^n_m = H^n, \tag{13}$$

where B, A, and H are the projections of β, α, and h on the staggered grid. For simplicity, B and A are time independent diagonal matrices, but H is a time dependent vector. In the case of unbounded regions, periodic and absorbing conditions could be easily implemented. For periodic conditions, an explicit expression will be developed in the next section. On the other hand, absorbing boundary conditions have multiple implementations in the technical literature, and their review will not be pursued here. In this article, we implement absorbing boundary conditions using techniques based on the one-way wave equation as in [17],

$$\frac{1}{cb}\frac{\partial u}{\partial t} + \frac{\partial u}{\partial n} = 0. \tag{14}$$

Here, cb is the wave velocity at the boundary. Mimetic discretization of the one way wave equations is

$$\frac{1}{CB}\frac{(U^{n+1}_m - U^n_m)}{\triangle t} + B^s_{nd}G^s_{nd}U^n_m = 0. \tag{15}$$

In this expression, $\frac{1}{CB}$ is the projection of $\frac{1}{cb}$ on the staggered grid and it is a diagonal matrix. A naive leapfrog time approximation in (14) turned out to be unstable on our implementations, so the forward time discretization is

adopted. Equations (13) and (15) represent the mimetic discretizations for general Robin's or absorbing conditions on any staggered cartesian uniform grid.

Spatial discretizations in (11) contain null rows associated to boundary conditions, corners, and edges. The superposition principle allow us to reduce the number of null rows by adding the mimetic discretizations of boundary conditions, (13) and (15), to the partial mimetic discretization of the acoustic wave equation (11). In the case of Robin's conditions, such superposition produces the following full mimetic scheme

$$\frac{1}{C^2}\frac{(U_m^{n+1}-2U_m^n+U_m^{n-1})}{\triangle t^2}-(D_{nd}^sG_{nd}^s-BB_{nd}^sG_{nd}^s-A)U_m^n=F^n+H^n. \tag{16}$$

For the absorbing boundary conditions, the superposition of (11) and (15) leads to the full mimetic scheme

$$\frac{1}{C^2}\frac{(U_m^{n+1}-2U_m^n+U_m^{n-1})}{\triangle t^2}+\frac{1}{CB}\frac{(U_m^{n+1}-U_m^n)}{\triangle t}-(D_{nd}^sG_{nd}^s-B_{nd}^sG_{nd}^s)U_m^n=F^n. \tag{17}$$

Equations (16) and (17) represent a new general second order mimetic scheme for the acoustic wave equation on cartesian uniform grids for two general types of boundary conditions. For $n>1$, the spatial discretization matrices of these equations still present some null rows. They are associated to boundary corners and edges required for the tensor product formulation, but they can be ignored in the new mimetic scheme.

In order to appreciate the new features of the proposed scheme, scalar equations comprised in (16) are next explicitly described in the one dimension case, $n=1$, on the grid given in figure 1. First equation represents the left boundary condition

$$\left(-\beta\frac{8}{3h}+\alpha\right)u_0^n+\frac{3}{h}u_{\frac{1}{2}}^n-\frac{1}{3h}u_{\frac{3}{2}}^n=h_0^n \tag{18}$$

that is a one side approximation with three terms requires for second order accuracy. Next equation at the first inner node is given by

$$\frac{1}{c_{\frac{1}{2}}}\frac{(u_{\frac{1}{2}}^{n+1}-2u_{\frac{1}{2}}^n+u_{\frac{1}{2}}^{n-1})}{\triangle t^2}-\left(\left(\frac{8}{3h^2}-\frac{1}{3h}\right)u_0^n+\left(\frac{1}{2h}-\frac{4}{h^2}\right)u_{\frac{1}{2}}^n+\left(\frac{4}{3h^2}-\frac{1}{6h}\right)u_{\frac{3}{2}}^n\right)=f_{\frac{1}{2}}^n \tag{19}$$

with accuracy of second order in time and first order in space. This spatial reduction of accuracy was expected from the non uniform distribution of staggered grid nodes near the boundary. Notice the unusual linear terms on h (in the denominators) for a laplacian approximation, and they come from the superposition of the boundary conditions. The equation associated to the second inner node takes the following expression

$$\frac{1}{c_{\frac{3}{2}}}\frac{(u_{\frac{3}{2}}^{n+1}-2u_{\frac{3}{2}}^n+u_{\frac{3}{2}}^{n-1})}{\triangle t^2}-\left(\left(\frac{1}{3h}\right)u_0^n+\left(\frac{1}{h^2}-\frac{1}{2h}\right)u_{\frac{1}{2}}^n+\left(\frac{1}{6h}-\frac{2}{h^2}\right)u_{\frac{3}{2}}^n+\left(\frac{1}{h^2}\right)u_{\frac{5}{2}}^n\right)=f_{\frac{3}{2}}^n. \tag{20}$$

This equation is also second order accurate in time and only first order in space. This first order of spatial accuracy is due to the four-point non symmetric laplacian approximation around $x_{\frac{3}{2}}$. After the second interior node, following discretizations correspond to the standard finite difference wave equation approximation

$$\frac{1}{c_{i+\frac{1}{2}}}\frac{(u_{i+\frac{1}{2}}^{n+1}-2u_{i+\frac{1}{2}}^n+u_{i+\frac{1}{2}}^{n-1})}{\triangle t^2}-\left(\left(\frac{1}{h^2}\right)u_{i+\frac{3}{2}}^n-\left(\frac{2}{h^2}\right)u_{i+\frac{1}{2}}^n+\left(\frac{1}{h^2}\right)u_{1-\frac{1}{2}}^n\right)=f_{i+\frac{1}{2}}^n. \tag{21}$$

They offer second order accuracy in both dimensions time and space. The equations associated to nodes $x_{n-\frac{3}{2}}$,$x_{n-\frac{1}{2}}$, and x_n are omitted because of they are symmetrical to equations (20), (19), and (18), respectively.

Scalar equations associated to the scheme (17) are identical to those described in (16), with the exception of boundary conditions. In this case, the left boundary condition becomes the mimetic discretizations of the one way wave equation

$$\frac{1}{cb_0}\frac{(u_0^{n+1}-u_0^n)}{\triangle t}-\frac{8}{3h}u_0^n+\frac{3}{h}u_{\frac{1}{2}}^n-\frac{1}{3h}u_{\frac{3}{2}}^n=0. \tag{22}$$

Above approximation is first order in time and second order in space. Equation at the right boundary is symmetric and its expression is also omitted. This description leads to an important fact of mimetic methods described in this article, namely, discretizations at inner nodes in mimetic schemes remains invariant under boundary condition changes. This observation allows us to write mimetic schemes (16) and (17) in a very general expression

$$\frac{1}{C^2}\frac{(U_m^{n+1}-2U_m^n+U_m^{n-1})}{\triangle t^2}+\left(\frac{1}{CB}\right)^*\frac{(U_m^{n+1}-U_m^n)}{\triangle t}-(D_{nd}^sG_{nd}^s-B^*B_{nd}^sG_{nd}^s-A^*)U_m^n=F^n+H^n. \tag{23}$$

Above matrices $(\frac{1}{CB})^*$, B^*, and A^* can always be chosen to incorporate a mixed set of boundary conditions. Notice that a leapfrog time discretization for the one-way wave equation implementing an absorbing boundary condition would lead to a simpler expression for (23). Unfortunately, this approximation triggers instabilities in our numerical experiments.

4. Convergence analysis

A convergence analysis of the general mimetic scheme (23), or its particular cases (16) and (17), is cumbersome because it would lead to consider too many cases, even for one dimensional problems. In fact, most convergence analyses of finite difference schemes are done on one dimensional problems under periodic boundary conditions. Such approach is applied here to the new mimetic scheme proposed in the previous section. Under periodic boundary conditions, the mimetic scheme for the one dimensional acoustic wave equation is defined by (16) for $A = 0$ and B becomes a diagonal matrix with ones at the boundary nodes and zeros elsewhere. For simplicity we also assume that $F = 0$, and then periodicity conditions are given by

$$\begin{aligned} u_0^j &= u_n^j \\ -\frac{1}{h}\left(\frac{8}{3}u_0^j-3u_{\frac{1}{2}}^j+\frac{1}{3}u_{\frac{3}{2}}^j\right) &= \frac{1}{h}\left(\frac{8}{3}u_n^j-3u_{n-\frac{1}{2}}^j+\frac{1}{3}u_{n-\frac{3}{2}}^j\right), \end{aligned} \tag{24}$$

where j represents a generic time step level. Next, conditions (24) are substituted into the discrete equations of the mimetic scheme at interior points $x_{\frac{1}{2}}$ and $x_{\frac{3}{2}}$, and lead to the following new expressions for the scheme's equations at these locations

$$u_{\frac{1}{2}}^{j+1}=\left(c\triangle t\right)^2\left(\left(\frac{5}{16h}-\frac{5}{2h^2}\right)u_{\frac{1}{2}}^j+\left(\frac{7}{6h^2}-\frac{7}{48h}\right)u_{\frac{3}{2}}^j+\left(\frac{3}{2h^2}-\frac{3}{16h}\right)u_{n-\frac{1}{2}}^j+\left(\frac{1}{48h}-\frac{1}{6h^2}\right)u_{n-\frac{3}{2}}^j\right)+2u_{\frac{1}{2}}^j-u_{\frac{1}{2}}^{j-1}, \tag{25}$$

and

$$u_{\frac{3}{2}}^{j+1}=(c\triangle t)^2\left(\left(\frac{1}{h^2}-\frac{5}{16h}\right)u_{\frac{1}{2}}^j+\left(\frac{7}{48h}-\frac{2}{h^2}\right)u_{\frac{3}{2}}^j+\left(\frac{1}{h^2}\right)u_{\frac{5}{8}}^j+\left(\frac{3}{16h}\right)u_{n-\frac{1}{2}}^j-\left(\frac{1}{48h}\right)u_{n-\frac{3}{2}}^j\right)+2u_{\frac{3}{2}}^j-u_{\frac{3}{2}}^{j-1}. \tag{26}$$

Mimetic discretizations at the last interior nodes, $x_{n-\frac{3}{2}}$ and $x_{n-\frac{1}{2}}$, take identical symmetric expressions as those given by (26) and (25), respectively. Thus, we omit their expresions. Collecting all these new equations along with those unchanged by the periodic boundary conditions, the mimetic scheme can be written as this vector formulation with three time levels

$$U_m^{j+1}=LU_m^j-U_m^{j-1}, \tag{27}$$

where $U_m^j\equiv(u_{\frac{1}{2}},u_{\frac{3}{2}},...,u_{i+\frac{1}{2}},...,u_{n-\frac{3}{2}},u_{n-\frac{1}{2}})^t$. L is a square matrix whose first three rows are explicitly given below. The last and penultimate rows of L are symmetric repetitions of its first and second ones, respectively, with their entries displayed in reverse order. That is,

$$L=\begin{pmatrix} 2+(\frac{5}{16h}-\frac{5}{2h^2})r^2 & (\frac{7}{6h^2}-\frac{7}{48h})r^2 & 0 & \cdots & \cdots & 0 & (\frac{1}{48h}-\frac{1}{6h^2})r^2 & (\frac{3}{2h^2}-\frac{3}{16h})r^2 \\ (\frac{1}{h^2}-\frac{5}{16h})r^2 & 2+(\frac{7}{48h}-\frac{2}{h^2})r^2 & (\frac{1}{h^2})r^2 & 0 & \cdots & 0 & -(\frac{1}{48h})r^2 & (\frac{3}{16h})r^2 \\ 0 & \frac{1}{h^2}r^2 & 2-(\frac{2}{h^2}) & \frac{1}{h^2}r^2 & 0 & \cdots & \cdots & 0 \\ \ddots & \ddots & \ddots & \ddots & \ddots & \ddots & \ddots & \ddots \end{pmatrix}, \tag{28}$$

where $r \equiv c\frac{\triangle t}{h}$.

Under the assumption that matrix L can be diagonalized, the three-level formulation (27) can be transformed into a new vector formulation with each entry corresponding to a second order difference equation. By standard arguments, this implies that the mimetic scheme under study is stable as long as the eigenvalues λ of L satisfy the condition $|\lambda| < 2$. An application of the Gerschgorin's theorem, [14, 16], proves that the stability condition becomes

$$c\frac{\triangle t}{h} < \frac{\sqrt{3}}{2}. \tag{29}$$

In Appendix B, we present a stability analysis for the standard finite difference scheme based on ghost points, and show that its stability condition, under periodic boundary conditions, is slightly more restrictive than (29).

Consistency of the scheme given by (16) follows immediately from the fact that leapfrog time discretization [16] and the mimetic elliptic discretizations in space [12, 13], are both consistent. Thus, the Lax-Richtmyer theorem guarantees the convergence of the new mimetic scheme [16].

5. Numerical results

This section presents three numerical tests to illustrate some of the advantages of the new mimetic scheme for the acoustic wave equation. The first test will assess the accuracy of the mimetic and finite difference schemes in a one dimension problem. The second test will show the versatility of the mimetic scheme to handle combinations of general boundary conditions stated in previous sections. Finally, the third test shows an application to compute seismic traces excited by a point source on a layered model. This last test is representative of seismic propagation problems on heterogeneous media of current interest in geophysics.

5.1. Test No. 1: A convergence test

This test considers a one dimensional acoustic wave equation with unitary velocity and a null source term on the space interval [0,1]. Its analytic solution is given before hand and takes the form $u(x,t) = cos(2\pi x)[sin(2\pi t) + cos(2\pi t)]e^{-37x}$. Boundary conditions are a non homogeneous Neumann condition at the left boundary, $x = 0$, and absorbing condition at the right boundary, $x = 1$. Their source terms are obtained by direct substitution of the analytic solution in the boundary conditions. The analytic solution represents an oscillating boundary layer at $x = 0$ with time. The solution of the described initial boundary value problem was approximated by the new mimetic scheme and the standard finite difference (FD) method based on ghost points. Numerical approximations were obtained by both methods under mesh refinement, starting with ten nodes and ending with a one hundred and twenty nodes grids. Time steps sizes were identical for both schemes. They were small, and away from the stability limit. All approximations were computed at the final time $t = 1$ and L_2 error are illustrated in figure 2. Table 1 shows that errors from the finite difference scheme are consistently higher than those obtained by the mimetic scheme. Since time approximation in both schemes is the same, then errors of these approximations are determined by the accuracy of the space discretization in the wave equation. On the other hand, slopes of the errors curves in figure 2 seem to indicate that the convergence rates of both scheme are equal. Evaluations of their slopes, reported in table 1, are nearly 1.8, which is below the nominal convergence. This common performance deficiency may be explained by the fact that the boundary layer problem subject to this test is actually a hard problem for both methods. Higher accuracy of the numeric scheme, indicate that the spatial mimetic discretization, in the context of boundary layer problems, is a better choice than standard finite difference based on the ghost points approach. Tests with well behaved solutions would produce a quadratic convergence rate, but in those cases the errors would be almost identical for both schemes. These results imply that the second order approximation of boundary conditions, in the new mimetic scheme, dominates or cancel its first order approximations in space of the acoustic wave equation at the nodes close to the boundary.

5.2. Test No. 2: A test with mixed boundary conditions

Combination of boundary conditions at different domain's edges is a relatively complex issue in standard finite difference methods. In fact, this weakness is one of the reasons to justify the use of finite element schemes. Our new mimetic method is based on finite difference approximations, but one of its features is a rigorous and robust

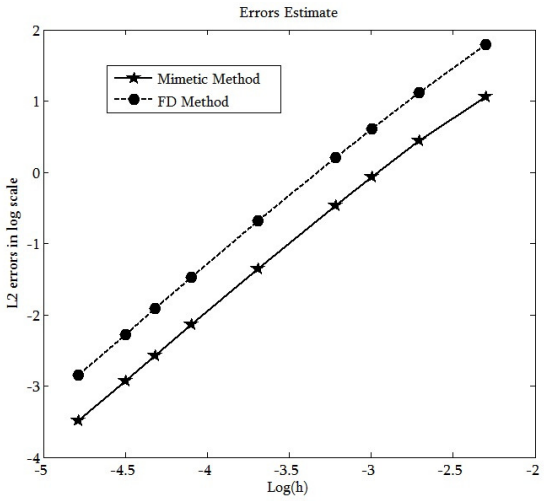

Figure 2: Test No. 1. Comparison of errors for mimetic and finite difference (FD) methods

Grid size	Error mimetic scheme	Error FD scheme
10	2.8774	6.0132
40	0.2572	0.5039
90	0.0535	0.1030
120	0.0307	0.0580
Rates	1.8811	1.8535

Table 1: Comparative table of L^2 errors and rates for Test No. 1

treatment of boundary conditions. This allows to implement a combination of boundary conditions without the complexity of standard finite difference or finite element methods. Such advantage was discussed from a theoretical and implementation point of view in previous sections, and the test given below illustrates the mimetic flexibility under a combination of three important boundary conditions. Now, let us describe the initial boundary value problem on the square domain $[0, 1] \times [0, 1]$, where the wave patterns depicted in figure 3, represent snapshots of the numerical solution. On the left boundary, $x = 0$, a homogeneous Dirichlet condition is enforced, and sometimes named as a fixed boundary condition [18]. On the opposite side, $x = 1$, a homogeneous Neumann's condition is set up, and represents a free boundary condition [18]. In this article, edges $y = 0$ and $y = 1$ are referred as front and back edges, respectively, and we impose absorbing boundary conditions on both of them. We also consider homogeneous initial conditions, set the wave speed to 1, and include a source term into the acoustic wave equation defined by the exponential function $Ae^{\beta(t-t_0)}$. Source parameters are the amplitude A, a shift time t_0 from $t = 0$, and β that controls the energy spectrum. This point source is placed at the center of the unit square meshed with an odd number of grid blocks, between four and five hundreds of cells along each direction, so the excited wavefront is completely symmetric. Analytic solutions for the described initial boundary value problem are unavailable, thus the following analysis is simply based on the physical qualitative behavior of the mimetic solution. Figure 3 shows three different snapshots of this solution. The display (a) depicts a distribution of the wavefront before it reaches any of the boundaries. It is completely circular and symmetric with respect to the square center with a bell-shaped amplitude. Since, this wavefront is a solution of the linear wave equation, it is expected that the initial Gaussian pulse spreads out in all radial directions. Panel (b) shows reflections of the circular wavefront, showed in (a), off boundary edges. Notice the high amplitude contrast between reflected waves from the back and front edges in comparison to the strong reflections from lateral boundaries $x = 0, 1$. It is well known that minor wave reflections from absorbing boundaries, based on one-way wave formulations, have a similar behavior to those observed from a free surface boundary, with a huge difference in amplitude. This is the exact behavior showed in panel (b). In fact, the negligible wave reflections from the back and front edges have amplitudes several orders of magnitude smaller than those waves reflected from the free surface at the right boundary. On

the other hand, waves reflected off lateral edges have approximately same amplitudes, as expected because mimetic schemes are conservatives. However, the crest of the direct wavefront has been transformed into a valley on the wave reflected by the left edge, as a consequence of the rigid-wall condition. Keep in mind that boundary values at this edge remains equal to zero because of the Dirichlet condition. In contrast, boundary values at the right edge change as function of position y and the reflected wave keeps the same amplitude crest of the incident wave. The display (c) gives evidence that reflected wavefronts move at the same speed, and tiny reflections from absorbing boundaries do not significantly affect the amplitude of these strong wavefronts. It is quite evident that wave reflections in panel (c) produce a characteristic flower structure commonly observed in numerical solutions of the acoustic wave equation with constant speed. Above results offer a strong indication that the new mimetic scheme can easily handle mixed boundary conditions, and computed solutions qualitatively satisfy the physics modeled by the acoustic wave equation.

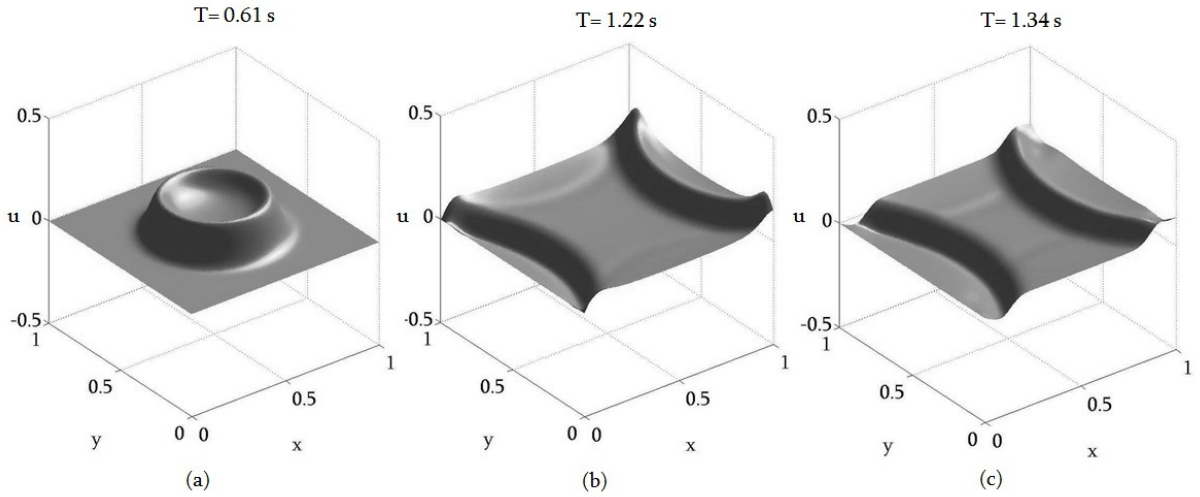

Figure 3: Test No. 2. Boundary conditions effects

5.3. Test No. 3: A heterogeneity test

Previous tests have assumed that the acoustic wave equation is solved in a medium with constant wave velocity. However, this assumption was just taken for convenience rather than being a limitation of the new scheme. A typical seismic imaging problem in geophysics consists in finding the underground material distribution of Earth, and the purpose of a seismic reflection survey is collecting wave traces in the field at near-surface receivers. In theory, geophysicists are able to induce the underground layering distribution by analyzing the P-wave component in seismic traces. P-wave components in seismic traces can be modelled by the propagation of compresional waves using the acoustic wave equation. In their simplest form, underground earth layers are identified by a sudden strong variation of the P-wave propagation speed. Therefore, the velocity parameter in the acoustic wave equation must vary in space, and this leads to a typical heterogeneous problem. Mathematically, modeling the underground propagation of P waves near the surface, by the acoustic wave equation, usually represents Earth by the lower $x - y$ half-plane with the topographic surface at its upper edge. For simplicity, earth surface is assumed to be flat. Application of volumen-discretization numerical methods to wave propagation problems on such idealized infinite domains require absorbing boundary conditions to limit the actual computational domain. In the technical literature, there are several numerical techniques for implementing absorbing boundaries, but in this paper we adopt an approach based on the one-way wave equation proposed in [17] to simulate P wave propagation using a standard finite difference method. We already used this type of conditions in previous test No. 2. Reynolds' paper presents several test problems on simple 2D domains with horizontal layering, and our third test is an adaptation of one of his heterogeneous problems for acoustic wave propagation. The setup for this test No. 3 is as follows: A square region with each side having length 9760 meters, and two horizontal layers. First layer has the topographic surface at one of its edges, and exhibits a vertical extension of 4880 meters, with wave speed 1500 meters/second. Second layer is also 4880 meter deep and

has a wave velocity of 4000 meters/second. The point source for P wave generation is located 740 meters below the surface in the first layer and centered with respect to lateral edges. We place the source at this location to have symmetry of the seismic traces. This heterogeneous test was solved by our mimetic scheme under two different sets of boundary conditions. First set forces wave amplitudes to zero at all four edges. The second set combines a null Dirichlet condition at the surface with absorbing conditions at remaining edges. We use our new mimetic scheme to compute numerical seismic traces on a 488×488 grid, and results for both sets of boundary conditions are shown in figure 4. Display (a) depicts after approximately 1.5 seconds of simulation, the wave pattern resulting from fixed boundary reflections. These results have no a seismic connotation, but are shown as a visual reference for the wave absorption implementation using Reynolds' conditions. Panel (b) depicts the expected behavior of seismic traces in a two-layered half plane. Notice that after 3 seconds, seismic traces show small reflections because of the low effectiveness of Reynolds' absorbing boundary conditions, and they must not be interpreted as a deficiency of the numerical scheme. Comparison of traces in figure 4 with the original ones reported in [17] are qualitatively identical. A further assessment of mimetic waveforms in panel (b) can be performed by means of ray tracing, that can be done analytically. However, this comparison is not included in this article for the sake of brevity.

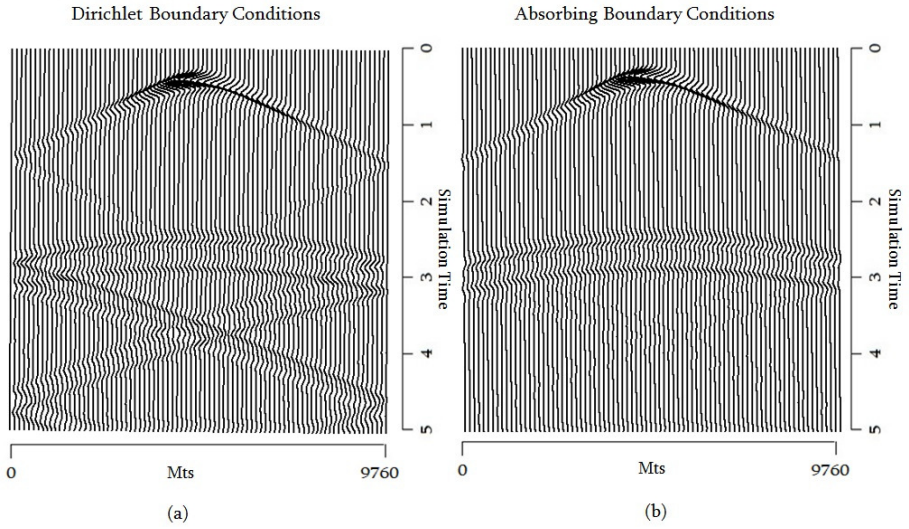

Figure 4: Test No. 3. Seismic traces computed by the new mimetic scheme in a layered model

6. Conclusions and discussion

This article presents a new and versatile mimetic scheme for the solution of acoustic wave in bounded and unbounded domains. Its multidimensional formulation based on tensor products is a new contribution in the context of mimetic operators described in [1, 12, 13]. Also, description of the mimetic discretization of gradient and divergence operators, in a multidimensional setting, is an additional contribution from the notational point of view. In particular, the multidimensional representation of the discrete Green-Gauss-Stokes' theorem is original and it certainly simplifies the description of the new mimetic scheme. A convergence analysis of the new mimetic scheme proves that it has a higher stability limit than the standard finite difference scheme based on ghost points, in one dimensional domains. Since, this new scheme in higher dimensions is formulated in terms of tensor products, then the upper bound in the one dimensional stability analysis can be generalized immediately for the multidimensional scheme. Combination of different boundary conditions can be easily implemented with the new mimetic scheme. Numerical results give evidence that the new mimetic scheme yields approximations to the solution of the acoustic wave equations that are qualitatively and physically correct. On tests where accuracy can be measured, mimetic approximations to exact solutions show good convergence rates that agree with the second order discretization of boundary conditions. Absorbing boundary conditions are implemented by using standard models based on the one-way wave equation. These conditions generate insignificant edge reflections in our numerical tests. Such reflections should not be interpreted as a

weakness of the new scheme, but rather a consequence of the low efficiency of the absorbing boundary conditions coupled to our mimetic scheme.

It is not clear, at this time, that the improvement of the stability condition achieved by the mimetic discretization of the acoustic wave equation can be attained by the application of same operators to other time dependent PDE's. This should be a topic of future studies.

Acknowledgement

Authors from Universidad Central de Venezuela (UCV) were partially supported by: Consejo de Desarrollo Científico y Humanístico de la UCV, Vice-rectorado Académico de la UCV, Coordinación de Investigación de la Facultad de Ciencias UCV, and Banco Central de Venezuela (BCV).

[1] J. Castillo, G. Miranda, Mimetic discretization methods, CRC Press, 2013.
[2] L. B. da Veiga, K. Lipnikov, G. Manzini, The mimetic finite difference method for elliptic problems, Springer, MSA 11, 2014.
[3] D. Justo, High order mimetic methods and absorbing boundary conditions, VDM Verlag, 2009.
[4] M.Shashkov, Conservative finite difference methods for general grids, CRC Press, 1996.
[5] J. B. Runyan, A novel higher order finite difference time domain method based on the Castillo-Grone mimetic curl operator with applications concerning the time-dependent Maxwell equations, Master's thesis in san Diego State University, 2011.
URL `http://hdl.handle.net/10211.10/1181`
[6] J. Hyman, M. Shashkov, Mimetic discretizations for maxwell's equations, Journal of Computational Physics 151(2) (1999) 881–909.
[7] O. Rojas, S. M. Day, J. Castillo, L. Dalguer, Modeling of rupture propagation using high-order mimetic finite-differences, Geophysics J. Int. 172 (2008) 631–650.
[8] G. Ely, S. Day, J. Minster, A support operator method for viscoelastic wave modeling in 3d heterogeneous media, Geophysical Journal International 172 (2008) 331–344.
[9] O. Rojas, R. Mellors, J. Castillo, Finite difference modeling of the P-SV wave equation with mimetic methods, Proceedings Society of Exploration Geophysics, 2003.
URL `http:dx.doi.org/10.1190/1.1817809`
[10] K. Lipnikov, L.Huang, A mimetic finite difference method for acoustic wave equations modeling on arbitrary meshes, Proceedings Society of Exploration Geophysics Annual Meeting, 2008.
[11] F. Solano-Feo, J. M. Guevara-Jordan, O. Rojas, An explicit mimetic method for transient beam equations, SVMNI (2012) MM43–MM48.
[12] J. E. Castillo, M. Yasuda, Linear systems arising for second-order mimetic divergence and gradient discretizations, Journal on Mathematical Modelling and Algorithms 4 (2005) 67–82. doi:10.1007/s10852-004-3523-1.
[13] J. Guevara-Jordan, S. Rojas, M.Freites, J. Castillo, Convergence of a mimetic finite difference method for static diffusion equations, Advances in Difference Equations 1 (2007) 1–12. doi:10.1155/2007/12303.
[14] J.W.Demmel, Applied numerical linear algebra, SIAM, 1997.
[15] M.R.Spiegel, Calculus of finite differences and differences equations, Schaum Outline Series, McGraw Hill, 1994.
[16] J. Strikwerda, Finite difference schemes and partial differential equations, SIAM, 2004.
[17] A. Reynolds, Boundary conditions for the numerical solution of wave propagation problems, Geophysics 43 (1978) 1099–1110.
[18] H. Young, R. Freedman, University physics with modern physics, Pearson, Addison Wesley, 2004.

Appendix A. One dimensional mimetic operators and quadrature weights

This appendix describes the matrix representation of the one dimensional (1D) mimetic operators formulated on the grid in figure 1. The 1D divergence operator corresponds to

$$D_{1d}^{n} = \frac{1}{h}\begin{pmatrix} 0 & 0 & \cdots & \cdots & 0 & 0 \\ -1 & 1 & 0 & \cdots & 0 & 0 \\ 0 & -1 & 1 & 0 & \cdots & 0 \\ 0 & 0 & \ddots & \ddots & 0 & 0 \\ 0 & \cdots & 0 & -1 & 1 & 0 \\ 0 & 0 & \cdots & 0 & -1 & 1 \\ 0 & 0 & \cdots & \cdots & 0 & 0 \end{pmatrix}_{(n+1)\times n}. \tag{A.1}$$

First and last zero rows are associated to the boundary nodes where the divergence is not defined.

The matrix expression for the 1D mimetic gradient operator is

$$G_{1d}^{n} = \frac{1}{h}\begin{pmatrix} -\frac{8}{3} & 3 & -\frac{1}{3} & 0 & \cdots & 0 \\ 0 & -1 & 1 & 0 & \cdots & 0 \\ 0 & 0 & \ddots & \ddots & 0 & 0 \\ 0 & \cdots & 0 & -1 & 1 & 0 \\ 0 & \cdots & 0 & \frac{1}{3} & -3 & \frac{8}{3} \end{pmatrix}_{n\times(n+1)}, \tag{A.2}$$

where stencils at the first and last rows represent the second order one sided gradient approximations to the exact gradient at both boundaries.

The 1D boundary operator defined by equation (6) takes the following form

$$B_{1d}^{n} = \begin{pmatrix} -1 & 0 & 0 & \cdots & & & 0 \\ \frac{1}{8} & -\frac{1}{8} & 0 & \cdots & & & \\ -\frac{1}{8} & \frac{1}{8} & 0 & \cdots & & & \\ 0 & 0 & 0 & \cdots & & & \\ \vdots & \vdots & \vdots & \ddots & \vdots & \vdots & \vdots \\ & & & \cdots & 0 & 0 & 0 \\ & & & \cdots & 0 & -\frac{1}{8} & \frac{1}{8} \\ & & & \cdots & 0 & \frac{1}{8} & -\frac{1}{8} \\ 0 & & & \cdots & 0 & 0 & 1 \end{pmatrix}_{(n+1)\times n}. \tag{A.3}$$

Notice that B_{1d}^{n} operator is dimensionless because the grid step h is absent.

The quadrature weights P and Q are diagonal matrices. In our formulation, Q corresponds to the identity and P takes the following form

$$P = \begin{pmatrix} \frac{3}{8} & 0 & 0 & 0 & \cdots & & 0 \\ 0 & \frac{9}{8} & 0 & 0 & \cdots & & \\ 0 & 0 & 1 & 0 & \cdots & & \\ \vdots & \vdots & \ddots & \ddots & \ddots & \vdots & \vdots \\ & & \cdots & 0 & 1 & 0 & 0 \\ & & \cdots & 0 & 0 & \frac{9}{8} & 0 \\ 0 & & \cdots & 0 & 0 & 0 & \frac{3}{8} \end{pmatrix}_{n\times n}. \tag{A.4}$$

Appendix B. Standard finite difference stability analysis

This appendix presents a standard finite difference approximation of the homogeneous acoustic wave equation, $f = 0$, under periodic boundary conditions on the 1D staggered grid depicted in figure 1. Boundary conditions are approximated by using ghost points. The formulation of this scheme can be fully described by only the equations at nodes x_0, $x_{\frac{1}{2}}$, and a generic inner grid point $x_{i+\frac{1}{2}}$. At x_0, the discrete equation is

$$u_0^{j+1} = 2u_0^j - u_0^{j-1} + \left(\frac{c\triangle t}{h}\right)^2\left(4u_{\frac{1}{2}}^j - 8u_0^j + 4u_{n-\frac{1}{2}}^j\right). \tag{B.1}$$

On the other hand, the finite difference approximation at $x_{\frac{1}{2}}$ corresponds to

$$u_{\frac{1}{2}}^{j+1} = 2u_{\frac{1}{2}}^j - u_{\frac{1}{2}}^{j-1} + \left(\frac{c\triangle t}{h}\right)^2\left(\frac{4}{3}u_{\frac{3}{2}}^j - 4u_{\frac{1}{2}}^j + \frac{8}{3}u_0^j\right), \tag{B.2}$$

while at an interior node $x_{i+\frac{1}{2}}$, the discretization is not affected by the approximations of boundary conditions and given as

$$u_{i+\frac{1}{2}}^{j+1} = 2u_{i+\frac{1}{2}}^j - u_{i+\frac{1}{2}}^{j-1} + \left(\frac{c\triangle t}{h}\right)^2\left(u_{i+\frac{3}{2}}^j - 2u_{i+\frac{1}{2}}^j + u_{1-\frac{1}{2}}^j\right). \tag{B.3}$$

Collecting all these equations, the finite difference scheme can be written as a three level vector formulation, similar to (27), but in this case, matrix L must have the following form

$$\begin{pmatrix} 2-8r^2 & 4r^2 & 0 & \cdots & \cdots & 0 & 4r^2 & 0 \\ \frac{8}{3}r^2 & 2-4r^2 & \frac{4}{3})r^2 & 0 & \cdots & \cdots & 0 & 0 \\ 0 & r^2 & 2-2r^2 & r^2 & 0 & \cdots & \cdots & 0 \\ \ddots & \ddots & \ddots & \ddots & \ddots & \ddots & \ddots & \ddots \end{pmatrix}. \tag{B.4}$$

Same comments apply to the last two rows of L as described in section 4 for the mimetic scheme. By Gerschgorin theorem, [14, 16], the stability condition for this scheme is

$$c\frac{\triangle t}{h} < \frac{1}{2}. \tag{B.5}$$